Geochemistry Geophysics Geosystems G3

Volume 14, Number 4
25 April 2013
doi:10.1002/ggge.20077
ISSN: 1525-2027

Published by AGU and the Geochemical Society

Constraining clay hydration state and its role in active fault systems

Anja M. Schleicher
University of Michigan, Department of Earth and Environmental Sciences, 1100 N. University Ave, Ann Arbor, Michigan, 48109-1005, USA (aschleich@umich.edu)

Heiko Hofmann
2-2475 West 3rd Avenue, Vancouver, BC, V6K 1L9, Canada

Ben A. van der Pluijm
University of Michigan, Department of Earth and Environmental Sciences, 1100 N. University Ave, Ann Arbor, Michigan, 48109-1005, USA

[1] To understand the role of hydrated clay minerals in active fault systems, a humidity chamber connected to an X-ray diffractometer was used to determine the adsorption of water onto and/or into the crystal structure of smectite. This new type of analysis was carried out under specific temperature and humidity conditions, using powdered clay size fractions (< 2 μm) of rock samples from the San Andreas Fault (USA) and the Nankai Trough (Japan). Pressure cannot be controlled, but does not significantly affect clay swelling at shallow conditions. Air-dried samples show a discrete smectite phase that swells after traditional ethylene glycolation to an interlayer distance of 1.5 and 1.7 nm. Using the humidity chamber, however, the samples show a shorter interlayer distance, between 1.09 and 1.54 nm. Based on our analysis, we show that (i) ethylene glycol overestimates the size of the interlayer space, and therefore water content, so is a crude maximum only; (ii) interlayer swelling occurs in smectite clay minerals at all temperatures between 25 and 95°C; and (iii) particle orientation increases with increasing humidity, indicating a higher mobility of smectite from interlayer hydration. Detailed characterization of the hydration state of smectite under original conditions is critical for understanding of clay-fluid interaction, the mechanical behavior during fault displacements, and fluid budgets at depth. We propose that humidity chamber experiments should be the new standard procedure to constrain swelling characteristics of natural and synthetic clay minerals.

Components: 7,400 words, 9 figures, 1 table.

Keywords: clay-hydration; SAFOD; NanTroSEIZE; smectite; humidity chamber.

Index Terms: 8045 Fractures and faults

Received 18 September 2012; **Revised** 28 January 2013; **Accepted** 28 January 2013; **Published** 25 April 2013.

Schleicher A. M., H. Hofmann, and B. A. van der Pluijm (2013), Constraining clay hydration state and its role in active fault systems, *Geochem. Geophys. Geosyst.*, *14*, 1039–1052, doi:10.1002/ggge.20077.

1. Introduction

[2] Smectite clay minerals, together with illite, chlorite, and mixed-layered clay minerals, are the most important low-temperature alteration products in fault rocks, and the presence of those hydrous aluminum phyllosilicates is increasingly evoked as controlling creep and slip in shallow sections of active fault systems [*Wu et al.*, 1975; *Schleicher et al.*, 2010; *Lockner et al.*, 2011; *Holdsworth et al.*, 2011; *Bradbury et al.*, 2011]. One key characteristic of smectite clay minerals is the ability to absorb interstitial water onto and/or into their crystal structure, which reduces the interparticle attraction and thus contribute significantly to their weakness. Many laboratory experiments have been carried out on smectite-rich rocks assessing the stick-slip and creep behavior of faults [e.g., *Saffer and Marone*, 2003; *Moore and Lockner*, 2007; *Morrow et al.*, 2007; *Ikari et al.*, 2009; *Carpenter et al.*, 2009, 2011; *Collettini et al.*, 2011].

[3] To understand the material behavior of a fault, and in particular the stick-slip behavior of smectite-bearing faults, it is crucial to investigate the characteristic clay minerals and their swelling performances. The identification of smectite and smectite mixed-layers relies on their basal reflections (*d*-spacing), which depends on the degree of water intake and the nature of the interlayer cations [e.g., *Laird*, 2006; *Drits et al.*, 1994]. The water molecules migrate into the interlayer space from the particle edges, attracted by the positively charged interlayer cations. Due to their dipole forces, they arrange around the cations and form, water layers. The most common cations in the interlayer space are Na^{+}, Ca^{2+}, or Mg^{2+}, which are able to substitute other cations in both the tetrahedral and octahedral positions [*Brindley and Brown*, 1980]. The cation substitution, as well as water uptake or release occurs easily due to changes in temperature, pressure, or fluid chemistry. Unless particular care is taken to control the temperature and humidity in the laboratory, the interlayer hydration is likely to be variable from layer to layer and the resulting basal reflections will not conform to integral orders of diffraction in accordance to Bragg reflection law.

[4] X-ray diffraction (XRD) analysis identifies smectite or mixed-layer smectite based on the shift of the characteristic (001) peak due to expansion or contraction of the interlayer space [*Moore and Reynolds*, 1997; *Brindley and Brown*, 1980]. *Bradley* [1945] and *Mac Ewan* [1948] showed that organic compounds, such as ethylene glycol, glycerol, and others, will enter the interlayer space and replace the water molecules in the interlayer space, which causes swelling. This radical displacement of molecules may give misleading data on swelling properties, resulting in the need for special sample preparation and X-ray analysis. In this paper, we propose a novel analysis to investigate the hydration behavior of smectite that combines X-ray diffraction analysis in a temperature-controlled hydration chamber, simulating natural in situ processes in the laboratory (Figure 1). Using this new approach, we quantify the hydration state of smectitic clay minerals, and its relation to temperature, depth, and fluid-rock chemistry. The properties have direct application to natural, clay-bearing fault rocks and synthetic samples used in laboratory experiments.

[5] We investigated smectite-bearing rocks from two different fault systems, the San Andreas Fault

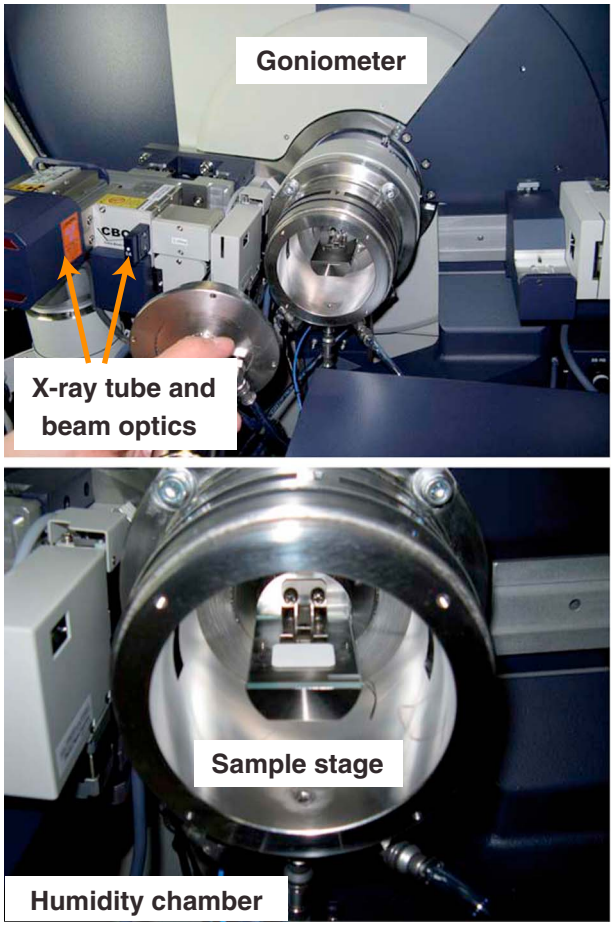

Figure 1. Setup of humidity chamber on a Rigaku XRD in Bragg-Brentano geometry. Textured sample was measured at constant RH and temperature after 30 min of acclimatization for each step. Measurement ranged between 2° and 14° 2θ and a step width of 0.02° 2θ, 2 s each step.

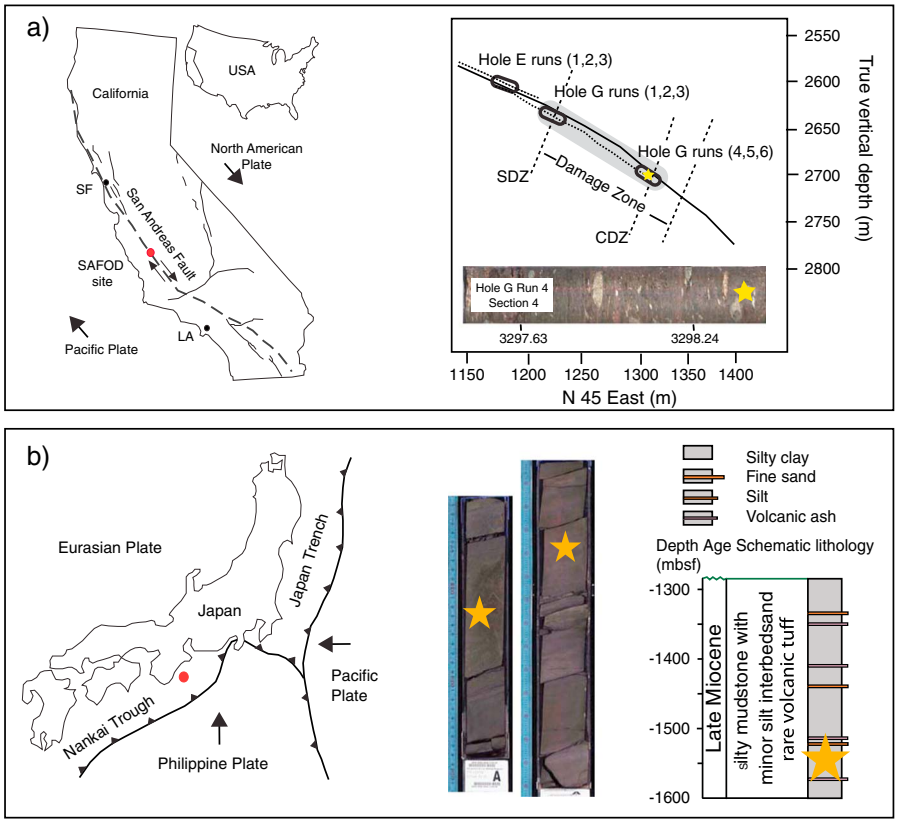

Figure 2. Map of study areas showing (a) locality of the SAFOD project site and borehole cross-section with sampling position and (b) locality of the NanTroSEIZE project site and borehole cross-section with sampling position

zone in western USA and the Nankai Trough subduction zone offshore Japan (Figure 2). The smectite formed authigenically in the actively creeping zone of the San Andreas Fault [*Schleicher et al*., 2010, 2012], whereas the smectite in the Nankai Trough belongs to clay-rich sediments and/or altered ash layers in the Kumano Basin and the slope of the underlying accretionary prism [*Kinoshita et al*., 2009; *Saffer et al*., 2010]. Because of their connection to active faulting and relatively high amount of smectite, these well-investigated areas offer a great opportunity to examine the properties of smectite clay minerals, to improve our understanding of strength and weakness of active faults, and to study the physical properties of faulting and earthquakes.

1.1. SAFOD and NanTroSEIZE Projects

[6] The San Andreas Fault is a ~1200 m long dextral transform fault in Central California with a history of earthquakes and creeping segments [*Agnew and Sieh*, 1978; *Hartzell et al*., 1996]. To address key issues of fault and earthquake mechanics, a ~3 km deep drillhole was drilled through the fault zone. The main hole was drilled to 3997 m measured depth (MD) [*Hickman et al*., 2004, 2008]. The drilling process ended in summer 2007 with Phase 3, producing cuttings and core from two actively creeping areas, referred as the southwest deformation zone (3196.4–3198.1 m MD) and the central deformation zone (3296.6–3299.1 m MD). These active fault traces are characterized by casing deformation [*Zoback et al*., 2011] and contain samples with notably low shear strength [*Carpenter et al*., 2011; *Lockner et al*., 2011]. The Nankai margin of southwestern Japan has a history of large earthquakes with major tsunamogenic potential [*Ando*, 1975; *Baba and Cummins*, 2005]. The NanTroSEIZE project was designed to create a distributed observatory spanning the updip limit of seismogenic behavior at a location where subduction earthquakes occur [*Tobin and Kinoshita*, 2006]. Several holes have been drilled along the Nankai margin to evaluate the aspects of seismogenic deformation. Expedition 319 includes two drill-sites (C0009 and C0010); site C0009 is located in the Kumano forearc basin, ~ 120 km away from the shore *Saffer et al*. [2010]. The drillhole is ~1600 m deep, and penetrates the Kumano Basin and the

underlying slope or accretionary prism [*Hayman et al.*, 2012]. Core was taken from 1509.7 to 1593.9 mbsf.

2. Methods

[7] Mineral assemblages were determined using a Rigaku Ultima IV XRD operating at 40 kV and 44 mA with Cu-Kα radiation. Bulk rock powder samples were measured for general mineral composition, and the < 2 μm fraction was separated for clay mineral analysis. Oriented samples were prepared and measured under air-dried and glycolated conditions. The resulting orientation of the platy clay particles allows their identification by measuring the Bragg-diffraction angle 2θ and the corresponding (atomic) layer distance in nanometers. A special humidity chamber was placed in the Rigaku Ultima IV XRD for humidity analysis (Figure 1). A thermocouple, heater cable and circulating water were connected to the attachment and the humidity generator. A circulating water tank controlled the temperature in the range between 30°C and 95°C. Temperature and humidity, as well as holding time, measure time, and measure range can be controlled by the specific computer software "TP2" from Rigaku. The samples were measured with Bragg-Brentano geometry between 2° and 10° 2θ for 2 s each step and a step-width of 0.02° 2θ. Each sample was measured in sequences from 10% relative humidity (RH) to 90% or 95% RH in steps of 10% or 20% RH, respectively, at $T = 25$, 50, and 75°C. The SAFOD sample was additionally measured at 90°C (see Table 1). To reveal the swelling behavior of both samples under controlled relative humidity and temperature conditions, the XRD profiles were decomposed using the peak fitting software MacDiff 4.2.5 [*Petschick*, 2010] with split-PearsonVII profile functions, and start values typical for discrete hydration states of swelling clay minerals (Figure 3). These are ~1.0 nm for dehydrated smectite, ~1.2 nm for 1-H_2O hydration state, ~1.5 nm for 2-H_2O, and ~1.7 nm for 3-H_2O state [*Moore and Reynolds*, 1997]. Based on these start values, the peak fitting software calculated possible compositions / overlaps of discrete phases allowing to vary intensity, peak position, and peak shape parameters automatically, until best fit was achieved. Resulting peak positions and intensities were plotted as a function of relative humidity and temperature. Error bars represent the standard deviation of 4 fitting calculations. Elemental geochemistry included the major rock forming elements Al^{3+}, Ca^{2+}, Fe^{2+}, K^{+}, Mg^{2+}, Na^{+}, and Ti^{2+}. Samples were analyzed using inductively coupled plasma-optical emission spectrometry (ICP-OES). The powdered rock samples (100 mg) were digested in 5% trace metal HNO_3 with 1 g of ultra-pure fused anhydrous lithium metaborate and 100 mg of lithium bromide. A Mn solution was used to align the ICP-OES, and calibrated using a blank and a certified high purity standard.

Table 1. Relative Humidity (RH), *d*-values (nm), Angle (Degrees 2θ), and Intensity (cps) Data of the SAFOD and NanTroSEIZE Sample Between 25 and 95°C

SAFOD					NanTroSEIZE				
T (°C)	RH (%)	*d*-value (nm)	Angle (° 2θ)	Intensity (cps)	*T* (°C)	RH (%)	*d*-value (nm)	Angle (° 2θ)	Intensity (cps)
25	20	1.26	7.00	4060	25	20	1.22	7.00	1295
	40	1.33	6.80	6430		40	1.23	7.00	1429
	60	1.36	6.50	8229		60	1.4	6.50	1645
	80	1.38	6.40	9913		80	1.41	6.10	1926
	95	1.40	6.40	10061		95	1.54	6.00	2028
50	20	1.12	7.80	1895	50	20	12.7	6.90	820
	40	1.29	6.80	2876		40	12.7	6.90	1002
	60	1.32	6.70	3687		60	12.9	6.80	1254
	80	1.35	6.50	4945		80	13.6	6.50	1401
	95	1.37	6.40	6106		95	13.9	6.40	1632
75	20	1.16	7.70	1268	75	20	12.6	7.00	601
	40	1.26	7.00	1680		40	12.6	7.00	706
	60	1.29	6.80	2161		60	12.7	6.90	854
	80	1.36	6.50	3021		80	12.7	6.90	923
	95	1.34	6.50	3624		95	12.8	6.90	1020
90	20	1.09	8.10	1071					
	40	1.21	7.10	1018					
	60	1.26	7.00	1477					
	80	1.29	6.80	1968					
	95	1.32	6.70	2156					

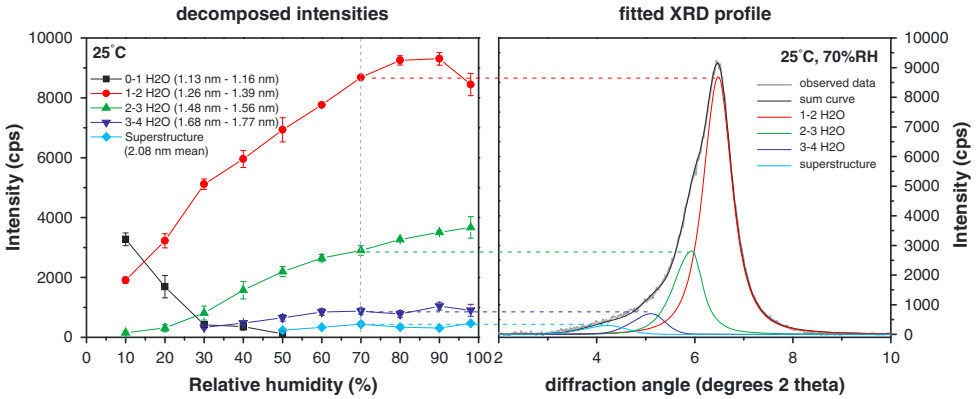

Figure 3. Example for the decomposing method based on SAFOD sample at 25°C and 70% RH. The measured XRD profiles show highly irregular peak shapes untypical for single phases. Peak decomposition reveals the presence of three or more hydration states and their transitions with time.

3. Results

3.1. Mineralogical and Chemical Composition

[8] The X-ray diffraction patterns of the clay size fraction (<2 μm) in samples from the active creeping zone in the San Andreas Fault and from the slope/accretionary sediments in the Nankai Trough show smectite peaks with characteristic peak positions that are changing from the air dried to the ethylene glycol state (Figure 4). The SAFOD sample reveals a smectite phase with a characteristic peak at 1.34 nm under air-dried conditions, which moves toward 1.52 nm after ethylene glycolization, indicating full swelling ability (Figure 4a). The clay mineralogy in the NanTroSEIZE sample is more complex, showing several overlapping peaks within the smectite phase under air-dried conditions, like chlorite (~1.46 nm) or illite-smectite (~1.1 nm) (Figure 4b). Illite is characterized by a peak at 1 nm, whereas kaolinite might overlap with chlorite at 0.71 nm. Bulk measurements additionally show quartz and minor pyrite in the clay size fraction (not shown here). After ethylene glycolization, the smectite phase moves to 1.7 nm, and the chlorite peak stays as a small hump at 1.4 nm, as expected. The chemical composition of the clay size fraction shows significant differences in the major elements, especially in Mg, Fe, and Ca (Figure 5). Mg and Fe are most abundant in the SAFOD sample with ~20 wt %, followed by Al (3.54 wt %), Ca (1.23 wt %), Na (0.28 wt %), and Ti (0.15 wt %). In the NanTroSEIZE sample, the elemental distribution is more homogeneous with 8.89 wt % Al, followed by Ca (3.97 wt %), Fe (4.25 wt %), K (3.01 wt %), Mg (1.31 wt %), Na (1.09 wt %), and Ti (0.35 wt %). The relatively high amount of K is probably due to the occurrence of illite, whereas Fe and Mg are most likely associated with chlorite.

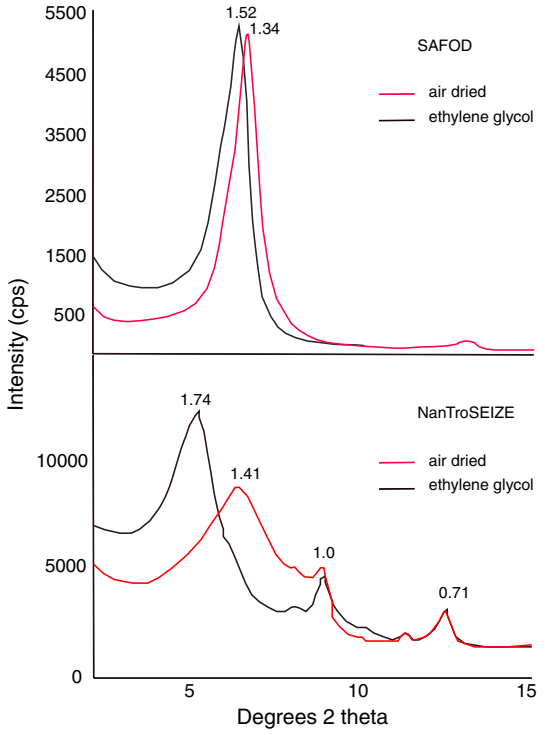

Figure 4. X-ray patterns of the clay size fraction: (a) Mg-rich smectite (saponite) from the SAFOD drillhole and (b) Ca-montmorillonite from the NanTroSEIZE drillhole.

3.2. Hydration State

[9] Figures 6 and 7 display X-ray diffraction patterns from the SAFOD and NanTroSEIZE samples at different temperatures (25, 50, 75, 95°C) and relative humidity (10–95%). At all temperatures, an increase in intensity and a peak-shift toward higher *d*-values (or lower °2θ values) are recognizable with

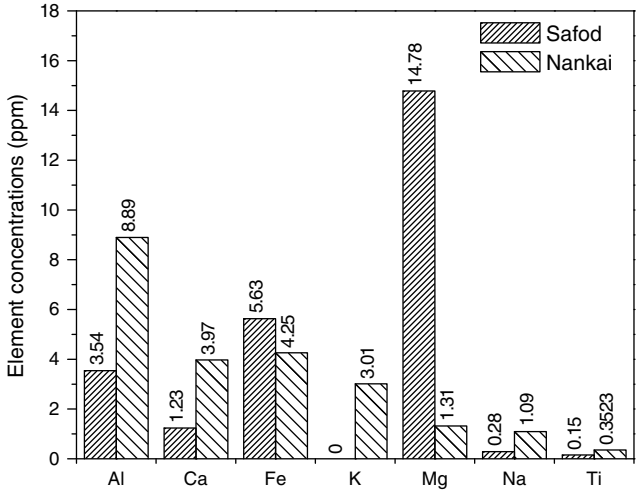

Figure 5. Chemical composition of an acidic digestion of the < 2 μm fraction using ICP-OES (a) of the SAFOD drillhole with Mg, Fe, Al, and Si as main constituents and (b) of the NanTroSEIZE drillhole with Ca, Fe, and K as main constituents.

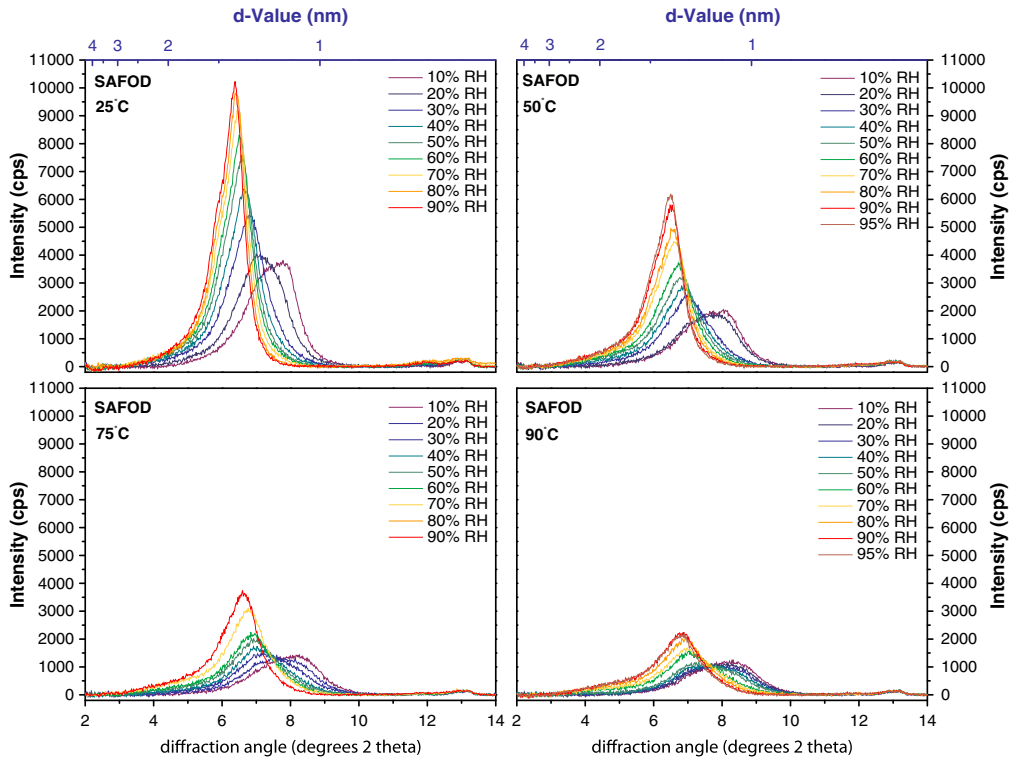

Figure 6. Humidity chamber analyses of the SAFOD samples: with increasing relative humidity the XRD peaks shift to higher *d*-values, indicating water uptake and swelling. At all temperatures the peak migration is accompanied by a strong increase in intensity.

increasing humidity. In the SAFOD sample, the patterns reveal homogeneous peaks between 25–90°C. At 25°C, the total intensity ranges from ~3500 to 10,000 cps, and the peak shifts from 1.1 to 1.4 nm (7.9 to 6.4 °2θ) with increasing relative humidity (Figure 6a). At 10% RH, the intensity is constant at ~3500 cps and the peaks are relatively broad with two peak maxima at 1.2/1.1 nm (7.2/7.9 °2θ). At 20–30 % RH, the peak becomes continuously thinner with only one peak maximum, whereas the intensity increases steadily to ~6000 cps. Between 40–95% RH, the intensity increases to ~10,000 cps, and the

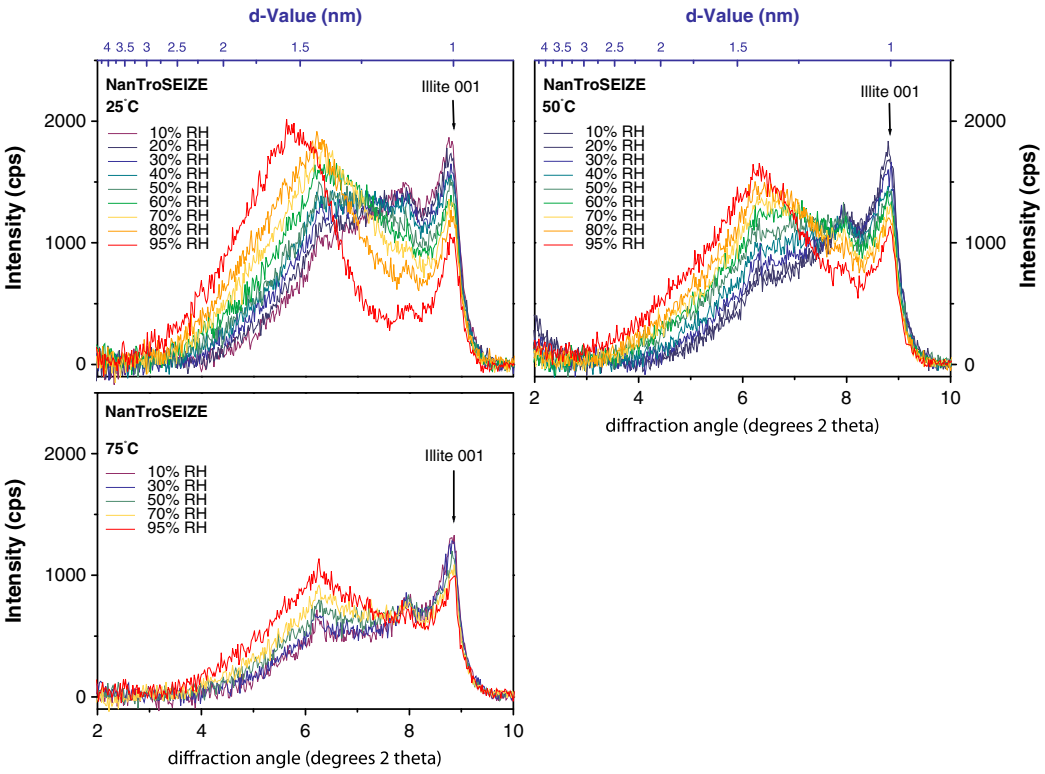

Figure 7. Humidity chamber analysis of the NanTroSEIZE sample.

peak shifts further to 1.4 nm (6.4 °2θ). At 50°C, the intensities range between ~2000 and ~6200 cps, and the peak shifts from 1.1 to 1.4 nm (7.9 to 6.4 °2θ) with increasing relative humidity (Figure 6b). The strongest increase can be recognized between 20–30% RH from 2000–2500 cps. At 75°C, the intensity is much lower than at cooler temperatures ranging between ~1500 cps and ~4000 cps, but the peaks shift from 1.07 to 1.36 nm (8.2 to 6.5 °2θ) with increasing relative humidity (Figure 6c). A slight decrease in intensity is recognizable between 10% and 20% RH, but then the increase in intensity with increasing humidity is homogeneous up to 4000 cps. At 10% RH the peak is situated at 1.07 nm (8.2 °2θ) and moves to 1.36 nm (6.5 °2θ) at 95% RH. The lowest intensities are recognizable at 90°C, ranging between 1200 and 2200 cps (Figure 6d). The peak shifts from 1.06 to 1.32 nm (8.3–6.7 °2θ). The intensity decreases slightly at 30% RH, but increases then continuously. One distinct peak shift occurs at 20% RH; afterward, the peak shifts continuously to 1.3 nm (6.7 °2θ).

[10] In the NanTroSEIZE sample, all XRD profiles show irregular peak shapes in comparison to a Gaussian-like shape for single phases, indicating an overlap or composition of more than two distinct phases or hydration states (Figures 7a–7c). In every profile a sharp peak at 1.0 nm (8.8 °2θ) can be observed. This peak is identified to reflect illite, a nonswelling clay mineral, because it does not change position with changing relative humidity. Another static peak was found at ~1.2 nm (8 °2θ) representing an illite/smectite mixed-layered clay mineral with minor swelling capability. Because the present illite peak position is not subject to position change under changing relative humidity conditions, it is used as internal standard for peak-shift corrections. At all temperatures, an increase in intensity and a peak-shift toward higher *d*-values (lower °2θ) are recognizable with increasing humidity. At 25°C, the peak intensity of the illite-smectite peak decreases from 1500 to 500 cps with increasing humidity; however, the peak itself does not shift toward higher *d*-values (lower °2θ). In contrast, the intensity of the discrete smectite peak increases continuously from ~1000 to ~1900 cps at humidity between 10–95% RH (Figure 7a). The peak shift of the smectite peak is more complicated. At 10% RH, a main peak is recognizable at 1.26 nm (7.0 °2θ). That peak becomes more pronounced between 30% RH and 40% RH, but stays at 1.26 nm (7.0 °2θ). At 50% RH, the peak shifts slightly from 1.26 to 1.27 nm (7.0 to 6.9 °2θ). Between 70 and 95% RH, two peaks are recognizable, with one main peak at 1.4 nm and a smaller peak at 1.3 nm (6.4 and 6.9 °2θ).

The highest *d*-value occurs at 95% RH with 1.48 and 1.4 nm (6.0 and 6.3 °2θ). At 50°C, the peak intensity is slightly lower in comparison to the peaks at 25°C (Figure 7b). Between 10–50% RH the peak intensity of illite-smectite stays at about 1300 cps, but decreases at 75% RH to 1100 cps, and to 900 cps at 90% RH. The intensity of the smectite peak decreases with increasing humidity from 1600 to 700 cps. The peak shift between 10 and 70% RH is not significant, and stays at 1.27 and 1.26 nm (6.9 to 7.0 °2θ). Between 80–95% RH, two peak maxima can be recognized, occurring at 1.36 and 1.26 nm (6.5/7.0 °2θ), and 1.39 and 1.26 nm (6.3/7.0 °2θ). At 75°C the illite peak decreases slightly at 95% RH and is otherwise very stable (Figure 7c). The smectite peaks range between 1.26 and 1.27 nm (~7.0 °2θ) between 10–70% RH. At 95% RH, two main peaks occur at 1.38 and 1.28 nm (6.4/7.0 °2θ).

3.3. Peak Decomposition

[11] At all temperatures in the SAFOD sample, the decomposed peak positions showed no values typical for discrete *n*-H_2O hydration states but intermediate values (Figure 8). These were classified as *n* to *n* + 1 H_2O hydration states with *n* = 0, 1, 2, 3, 4. Additionally, the formation of a superstructure (regular 1:1 interstratification of two phases) was observed over 50% and 70% relative humidity with a peak position at ~2.1 nm. Two major observations were made: The most dominant hydration state is the 1–2 H_2O state, which showed an increase in intensity from ~2000 cps at 10% RH to ~9500 cps at 90% RH at 25°C. At 50°C the intensities start at

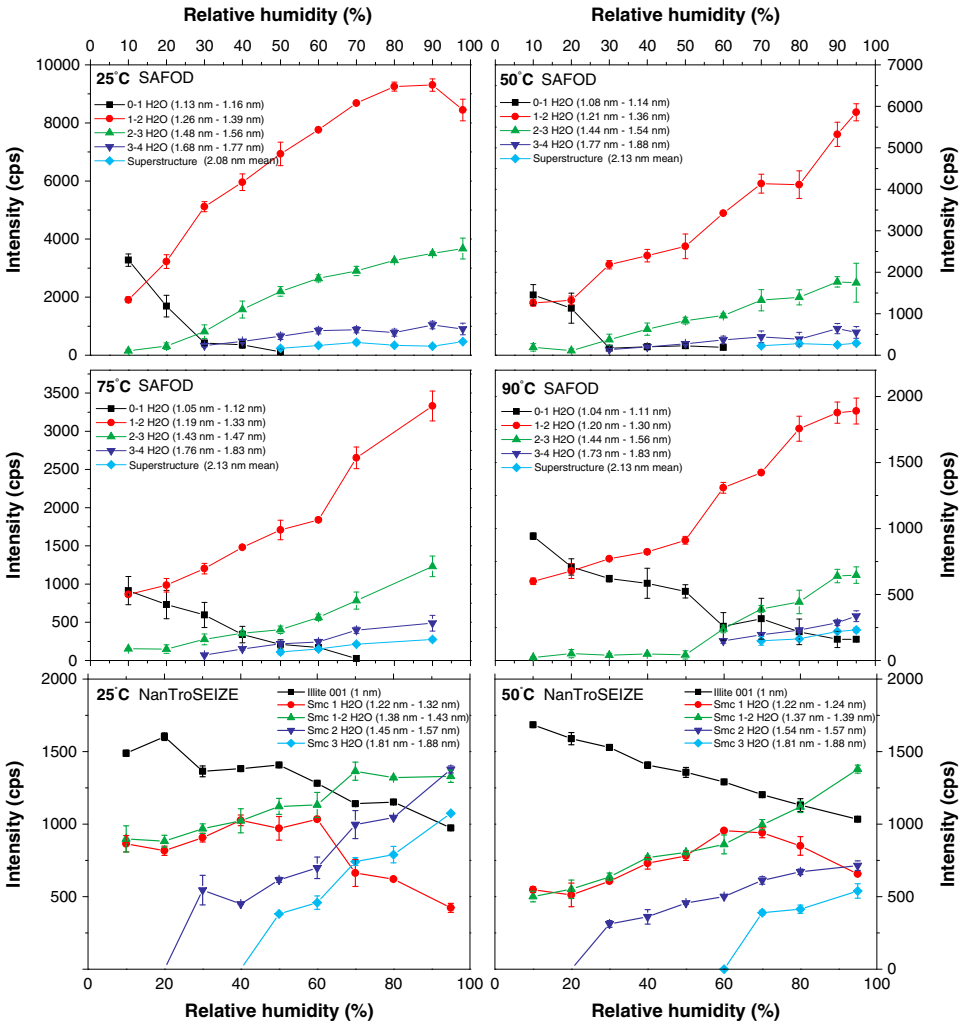

Figure 8. Decomposed peak intensities (cps) plotted against relative humidity based on the SAFOD and NanTroSEIZE samples.

~1800 cps increasing up to ~6000 cps, from ~800 to ~3300 cps at 75°C and from ~800 to 1800 cps at 90°C. Simultaneously, the 0–1 H_2O hydration state decreases at all temperatures and is being replaced by higher hydration states with increasing relative humidity. Only at 90°C some Mg-rich smectite (saponite) interlayers seem to remain unhydrated or hydrated with one water layer only. All other higher hydration states develop increasingly with increasing relative humidity, but not as dominant as the 1–2 H_2O state and without replacing each other. However, with increasing temperature it takes higher hydration states longer (at higher relative humidity) to develop.

[12] Analogous observations were made for the NanTroSEIZE sample (Figure 8). In contrast to the SAFOD sample, rather discrete hydration states for 1-H_2O, 2-H_2O, and 3-H_2O formed with increasing relative humidity. Only one intermediate state of 1–2 H_2O developed in addition, which again plays a dominant role over the other states. Additionally, a decrease of intensity of the internal illite standard with increasing relative humidity and increasing temperature was observed, which is caused by an increase of internal atomic-scale motion. At 25°C the intensity of the 1-H_2O state remains stable at ~800 to ~1000 cps and decreases down to < 500 cps above 60% relative humidity. At 50°C it increases slightly up to ~900 cps until 60% relative humidity and then decreases again. Only at 75°C it develops similar to the intermediate state of 1–2 H_2O and increases with increasing relative humidity. The higher hydration states of 2-H_2O and 3-H_2O kick-in at 20% relative humidity and 40% relative humidity, respectively (25°C), 20% and 60% relative humidity (50°C), and 30% and 70% relative humidity, respectively, at 75°C and then increase consequently.

4. Discussion

4.1. Mineralogical Effects During Clay Hydration

[13] Hydration and dehydration of smectitic clay minerals is a complex process at the crystal scale that involves constant reorganization of water within interlayers [*Ferrage et al.*, 2007a, 2007b]. The relative amount of this water is, among others, a function of the interlayer cations. These cations modify the surface area of the smectite and create water complexes in the interlayer, which differ in number of molecules and/or their spatial disposition [*Cuadros*, 1997]. The two smectite phases taken from the SAFOD drillhole and the NanTroSEIZE drillhole contain primarily Mg^{2+} and Ca^{2+} interlayer cations, respectively. Both phases react quickly to changing environmental conditions, and display a wide range of hydration states strongly depending on surrounding temperature and relative humidity. The Mg-rich smectite phase (saponite) from the SAFOD drillhole shows a relatively systematic increase of water layers with increasing humidity, ranging from 1 to max. 2–3 water layers. After *Cuadros* [1997], the cations promoting two water layers are Mg^{2+}, Ca^{2+}, and Sr^{2+}. Mg is smaller than Ca and so is its *d*-spacing, although the number of water molecules per half formula unit remains similar to Ca. It seems that for Mg the same number of water molecules is confined in a smaller volume due to its higher charge to radius ratio. The Ca-rich smectite from the

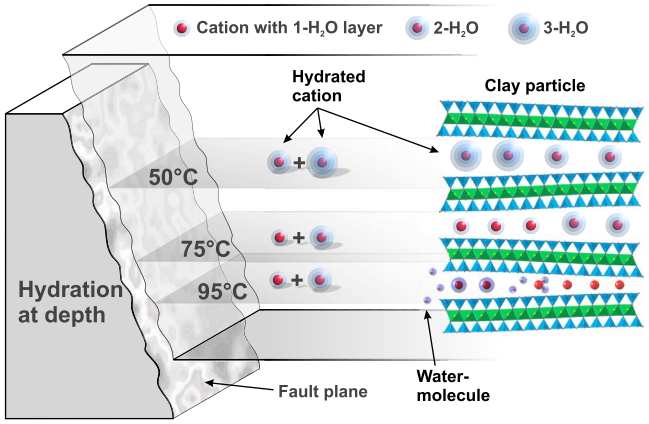

Figure 9. Schematic figure of smectite showing the process of swelling in a fault zone at depth. With decreasing water content the interlayer space and lattice distances decrease. Mixtures of two adjacent (or more) hydration states of different proportions are possible, resulting in transition states and peak positions between the positions of discrete hydration states.

NanTroSEIZE drillhole behaves more heterogeneously in developing water layers in the interlayer spaces. However, the smectite shows always two water layers between 25 and 75°C. *Iwasaki and Watanabe* [1988] and *Mooney et al*. [1952] showed that Ca-smectite forms the two water layers at 20% RH, whereas increasing humidity makes the *d*-spacing increase only slightly. This is likely due to water adsorption on the external surface, but it is also possible that more water molecules are incorporated to fill up the water structure that is already existent in the interlayer.

4.1.1. Influence of Relative Humidity

[14] Both Mg-rich smectite from the SAFOD drillhole and NanTroSEIZE Ca-montmorillonite swell with increasing relative humidity and temperature. However, the water uptake does not occur stepwise from one to the next higher hydration state. Except the lowermost 0–1 H_2O state for the SAFOD sample, and the 1 H_2O state for the NanTroSEIZE sample, all hydration states exist simultaneously with preferably 1–2 water layers. This means that different hydration states coexist and the interlayers are filled with water molecules continuously to a maximum of three water layers. The interlayer cations close to the crystal edges hydrate first while the ones further from the edges hydrate later. When water molecules reach the innermost cations to form the first or second water layer, the ones at the edges form the second and third state. Therefore, one single interlayer can contain more than one discrete hydration state, and an intermediate *d*-spacing will be measured by the X-ray diffractometer. Higher temperatures make the water migration into the interlayers more difficult. Interestingly, the intensities of the different hydration states (phases) also increase with increasing relative humidity. Because XRD intensity or peak height is, among other parameters, a function of the number of parallel crystal layers involved in scattering the X-rays [*Moore and Reynolds*, 1997], the number of the relative amount of layers is expected to decrease with increasing water content because water molecules cannot scatter X-rays and the penetrated volume stays the same. This is visible in the illite peak of the NanTroSEIZE sample, where the relative intensity decreases with increasing relative humidity. The relative content of smectite increases due to its increasing volume, whereas the illite volume does not increase. The only parameter that may be responsible for the increase of peak intensity of the smectite phases is the preferred orientation of the particles, which increases with the relative humidity. Here the water molecules increase the distance of the interlayer space, which accordingly decrease the attracting forces between the layers. This allows the crystal particles to rearrange and self-optimize preferred parallel orientation and therefore increases scattered intensity.

[15] The investigation of the swelling behavior in smectite in a closed system under controlled humidity and temperature conditions makes our analyses unique. Measuring the hydration state of smectite using a desiccator filled with water or saltwater usually shows an inaccurate range of water saturation depending on the temperature. Also, ethylene glycol that was used to identify smectite or smectitic mixed-layers, exaggerated the space of the interlayers due to the size of the molecules [*Hsieh*, 1989; *Mosser-Ruck et al*., 2005]. The reason for the different swelling behavior in the SAFOD and the NanTroSEIZE samples could be different interlayer cation compositions or layer charge characteristics caused by the unique substitution in the octahedral and tetrahedral layers. The swelling capability could also be affected by processes like alteration or heating. With the humidity chamber, both smectite phases have 1–2 water layers as preferred hydration states at temperatures between 50 and 95°C, which allows meaningful estimates of the water than can be expelled during dehydration.

4.1.2. Influence of Temperature and Pressure

[16] At all temperatures and relative humidity levels, the 1 or 1–2 water layer state are the preferred hydration states. The XRD profiles show a strong reduction of absolute intensity of both the sum curve and the decomposed single phases with increasing temperature. This is a well-known effect observed in XRD profiles caused by an increase of internal atomic-scale motion or oscillation of the electrons with increasing temperature and therefore reducing scattering efficiency [*Klug and Alexander*, 1974; *Brindley and Brown*, 1980]. The effect is reversible with decreasing temperature, and has no permanent effect on the material like breaking bonds, destruction of structure or permanent removal of interlayer water (collapse). Another important observation is the strong increase of hydration with temperature and relative humidity values, which is interpreted to be more difficult to form higher hydration states at higher temperatures.

[17] In our experiments, we could not measure water uptake as a function of pressure. However,

it is known that hydration can induce high swelling pressures for different hydration states, when the surrounding volume is limited [*Mueller-Vonmoos and Kohler*, 1993]. This is due to the fact that the hydration energy of interlayer cations is much higher than the forces that attract the particles. Theoretically, swelling pressures of more than 100 MPa can occur, and for a Wyoming bentonite (Na-montmorillonite) a pressure of up to 400 MPa was calculated, while forming the first hydration state. For the second hydration state, a swelling pressure of 110 MPa, and for the third, 27 MPa was calculated. All values are based on the adsorption isotherms of montmorillonite [*Mueller-Vonmoos and Kohler*, 1993]. These numbers appear high compared to the work carried out by *Tessier et al*. [1998] or *Bird* [1984], and are above the effective stresses acting on these faults. *Bird* [1984] showed in a hydration phase diagram from the Gulf Coast that two water layers can occur in Ca-montmorillonite at 3 km depth with pressure conditions of ~60 MPa (lithostatic) and ~30 MPa (hydrostatic), whereas one water layer occurs in Na-montmorillonite under the same conditions. He claims that transitions occurring at 300–6000 m depth with hydrostatic pressures are depressed to greater depths by superhydrostatic pressures, but the temperature gradient restricts this depression to about half of that predicted by the isothermal "effective pressure" concept.

[18] The Mg-rich smectite sample from the San Andreas Fault was taken at ~2.7 km depth, reflecting a pressure of ~80 MPa assuming a general gradient of 30 MPa/km, whereas the sample from the Nankai Trough was taken at ~1.6 km depth, reflecting ~48 MPa. This means that, theoretically, smectite in the Nankai Trough is able to take 2–3 water layers into their interlayer sheets, and smectite in the San Andreas Fault two water layers. The fact that there are two water layers in both samples shows that the limiting factor is rather temperature and/or cation exchange, but not pressure. Therefore, we conclude that the materials examined here record the hydration states at depth in the same way as we observed swelling under our laboratory conditions.

4.2. Clay Hydration and Implications for Frictional Strength

[19] Constraining the water content in SAFOD and NanTroSEIZE samples, it is essential to understand the effect of the hydration state of smectite and its influence on the environment. Following *Bird* [1984] and *Ikari et al*. [2007], we describe the hydration state of Ca-montmorillonite and Mg-smectite based on the number of water interlayers. In the one water layer hydration state, the cation is surrounded by four water molecules, two water layers contain six water molecules, and with three water layers the interlayer cation is surrounded by > 6 water molecules that are randomly oriented around the cation. Using the empirical formula $Na_{0.2}$ $Ca_{0.1}$ ($Al_{1.6}$, $Mg_{0.4}$) Si_4 O_{10} $(OH)_2$ for Ca-montmorillonite (taken from MinDat.org), the molecular weight is 367.4 g/mol, plus 18 g/mol for water. Assuming a mixture of Na^+ and Ca^{2+} in the interlayer space and a layer charge of 0.4, dry layers contain < 3.3 wt % water, whereas one water layer arrangements contain 4.4–5.9 wt %, two water layers 7.5–8.8 wt %, and three water layers contain 8.8 wt % of water. With the empirical formula $Ca_{0.16}$ ($Mg_{2.67}$ $Al_{0.33}$) ($Si_{3.34}$ $Al_{0.66}$) O_{10} $(OH)_2$ for Mg-smectite [*Moore and Reynolds*, 1997], the molecular weight is 405 g/mol and 18 g/mol for water. Assuming solely Ca^{2+} in the interlayer space and a layer charge of 0.3 for saponite, dry layers contain < 2.9 wt % water, one water layer arrangements contain 4.4–5.9 wt %, two water layers 7.30–8 wt %, and three water layers >8 wt % water. The values for Ca-montmorillonite from *Ikari et al*. [2007] and *Bird* [1984] are slightly different, reflecting Ca-montmorillonite with a different chemical composition. Although Mg- and Ca-smectite have different structural cation substitutions, they typically have the same layer charge of 0.3–0.4 charges per half unit cell. For this reason, they are comparable regarding their swelling ability.

[20] When smectite reaches equilibrium with the surrounding environment, the water content in the clay depends mostly on temperature and fluid availability. Even though the amount of water layers decreases from 2–3 to 1–2 water layers with increasing temperature in both the SAFOD and the NanTroSEIZE sample, there are still 1–2 water layers at 75°C and 95°C, reflecting up to ~8 wt % of water (Figure 9). However, controversial results exist about the stability of water layers at different depth and temperatures. For example, *Fitts and Brown* [1999] argue that smectite does not contain more than two layers of water with an effective stress as low as ~1.3 MPa, and, after *Colten-Bradley* [1987], interlayer water content reduces to one layer at 67–81°C, and the remaining layer is expelled at 172–192°C. The SAFOD sample belongs to an actively creeping section of the San Andreas Fault at ~3298 m MD with a temperature of ~112°C [*Bradbury et al*., 2011; *Williams et al*., 2004]. We observed 1–2 water layers at 95°C in the SAFOD

sample (Figure 6). Although lithostatic pressure condition at ~3 km depth could not be reproduced in our experiments, smectite swells at this depth with pressures up to 110 MPa for the second hydration state [*Mueller-Vonmoos and Kohler*, 1993], negating significant lithostatic pressure effects. The Ca-montmorillonite from the NanTroSEIZE drillhole C0009 was taken at a depth of ~1600 m below sea floor, showing temperatures of ~48°C [*Saffer et al.*, 2010; *Harris et al.*, 2011]. We observed 2–3 water layers at 50°C, which is a temperature ideal for the occurrence and formation of hydrated smectite.

[21] To understand the strength of a crustal fault, the investigation of the frictional properties of a fault gouge is crucial, and the swelling capacities of smectite that forms within the fault gouge. It is generally accepted that the amount of water in smectite interlayers lowers the frictional strength of a fault [e.g., *Bird*, 1984; *Moore and Lockner*, 2007; *Morrow et al.*, 2007; *Saffer and Marone*, 2003]. *Ikari et al.* [2009] showed the systematics of frictional behavior of montmorillonite-quartz gouge over a wide range of conditions, including water content, applied normal stress, clay content, and sliding velocity. Based on a combination of frictional strength experiments and our observations that smectite can contain interlayer water at depth, we conclude that water content in smectite has a very profound effect on the strength of faults at depth. However, the onset of seismic behavior is much more complicated and requires a combination of all those conditions including the content of other minerals in the fault gouge, clay hydration-dehydration processes, sliding velocities, and pressure and stress state. To determine the relative importance of those factors, more experiments are needed.

5. Conclusions

[22] Smectite is a common mineral in shallow fault rocks, with Mg-rich smectite dominating in the SAFOD drillhole and Ca-smectite dominating in the NanTroSEIZE drillholes. Both sampling areas investigated in this study are associated with active faulting processes, but formed under different environmental conditions. We demonstrate that carefully controlled humidity chamber experiments offer a more reliable measure of hydration state of smectite than traditional impregnation methods; the latter tend to overestimate the hydration capability of clay.

[23] Based on our experiments, we conclude that (i) smectite water layers occur at the depths where these rocks are sampled, (ii) the degree of hydration state at a given humidity is (relatively) unaffected by temperature up to 75°C–90°C, (iii) particle orientation increases with increasing humidity, suggesting higher mobility of the smectite particles cause by the hydration of interlayer cations. The quantification of hydration state of natural smectite is critical for our understanding of clay-fluid interaction and mechanical properties during fault displacements. Our new approach allows much more reliable determination of water layers in natural clays that can be used to determine mechanical properties in more realistic laboratory friction experiments and provide estimates of the volume of water released during dehydration at depth.

Acknowledgments

[24] The National Science Foundation (EAR-0738435 and EAR-1118704) and the Deutsche Forschungsgemeinschaft DFG (SCHL 1821/1-1 and 1–2) provided financial support for this fault rock research. We thank our many SAFOD and NanTroSEIZE colleagues (especially NanTroSEIZE Expedition 319) for many stimulating and challenging discussions, especially on the importance of clays in fault behavior. Special thanks to Jamie Gleason and Joel Blum, both at the University of Michigan, for ICDP-OES analysis. Two anonymous reviewers are gratefully thanked for their helpful comments.

References

Agnew, D. C., and K. Sieh (1978), A documentary study of the felt effects of the great California earthquake of 1857, *Bull. Seismol. Soc. Am.*, *68*(6), 1717–1729.

Ando, M. (1975), Source mechanisms and tectonic significance of historical earthquakes along the Nankai Trough, Japan, *Tectonophysics*, *27*(2), 119–140, doi:10.1016/0040-1951(75)90102-X.

Baba, T., and P. R. Cummins (2005) Contiguous rupture areas of two Nankai Trough earthquakes revealed by high resolution tsunami waveform inversion, *Geophys. Res. Lett.*, *32*(8), L08305, doi:10.1029/2004GL022320.

Bird (1984) Hydration-phase diagrams and friction of montmorillonite under laboratory and geologica conditions, with implications for shale compaction, slope stability, and strength of fault gouge, *Tectonophysics*, *107*, 235–260.

Bradbury, K. K., J., Evans, J. S., Chester, F. M., Chester, and D. L. Kirschner (2011), Lithology and internal structure of the San Andreas fault at depth based on characterization of Phase 3 whole-rock core in the San Andreas Fault Observatory at Depth (SAFOD) borehole, *Earth and Plan. Sci. Lett.*, *310*, 1–2, 131–144.

Bradley W. F. (1945), Molecular association between montmorillonite and some polyfunctional organic liquids, *J. Am. Chem. Soc.*, *67*, 975–981.

Brindley G. W., and G. Brown (1980), X-ray diffraction procedure for clay mineral identification, in Crystal Structures of clay minerals and their X-ray identification, edited by G. W. Brindley and G. Brown, Mineralogical Society, London, pp. 495.

Carpenter, B. M., C., Marone, and D. Saffer (2009), Frictional Behavior of Materials in the 3D SAFOD Volume, *Geophys. Res. Lett.*, *36*, L05302. doi: 10.1029/2008GL036660.

Carpenter, B. M., C., Marone, and D. M. Saffer (2011), Frictional strength of the san andreas fault from laboratory measurements of SAFOD drill samples, *Nat. Geosci.*. 10.1038/ngeo1089.

Collettini, C., A., Niemeijer, C., Viti, S. A. F., Smith, and Marone C. (2011), Fault zone fabric and fault weakness, *Earth and Plan. Sci. Lett.*, *311*, 316–327. 10.1016/j.epsl.2011.09.020.

Colten-Bradley, V. A. (1987), Role of pressure in smectite dehydration: effects on geopressures and smectite-to-illite transformation, *Am.Assoc.Pet.Geol.Bull.*, *71*, 1414–1427.

Cuadros, J. (1997), Interlayer cation effects on the hydration state of smectite, *Am. J. Sci.*, *297*, 829–841.

Drits, V. A., T. V., Varakina, B. A., Sakharov, and A. Plancon (1994), Simple technique for identification of one-dimensional powder x-ray diffraction patterns for mixed-layer illite-smectites and other interstratified minerals, *Clays and Clay Miner.*, *42*(4), 382–390.

Ferrage, E., C. A., Kirk, G. Cressey, and J. Cuadros (2007a), Dehydration of Ca-montmorillonite at the crystal scale, Part I: Structure evolution, *Am. Mineral.*, *92*, 994–1006.

Ferrage, E., B., Lanson, B. A. Sakharov, N., Geoffroy, E., Jacquot, and V. A. Drits (2007b), Investigation of dioctahedral smectite hydration properties by modeling of X-ray diffraction profiles: Influence of layer charge and charge location, *Am. Mineral.*, *92*, 1731–1743.

Fitts, T. G., and K. M. Brown (1999), Stress-induced smectite dehydration: ramifications for patterns of freshening and fluid expulsion in the N. Barbados accretionary wedge, *Earth Plan. Sci. Lett.*, *172*, 179–197.

Harris, R. N., F., Schmidt-Schierhorn, and G. Spinelli (2011), Heat flow along the NanTroSEIZE transect: Results from IODP Expeditions 315 and 316 offshore the Kii Peninsula, Japan, G-cube, *12*, 8. doi:10.1029/2011GC003593.

Hartzell, S. H., P. Liu, and C. Mendoza (1996), The 1994 Northridge, California, earthquake: Investigation of rupture velocity, rise time, and high-frequency radiation, *J. Geophys. Res.*, *101*(B9), 20091–20108.

Hayman N. W., T., Byrne, K., Kanagawa, K., Toshiya, C. M., Browne, A. M., Schleicher, G., Huftile, and L. McNeill (2012), Core constraints on the structural evolution of the inner wedge and sub-forearc basin, Nankai margin, Japan, *Earth Plan. Sci. Lett.*, *353–354*, 163–172.

Hickman, S., et al. (2008), Structure and composition of the San Andreas fault in central California: Recent results from SAFOD sample analyses: EOS (Transactions, American Geophyscal Union), 89, Fall meeting supplement, TT53F-01.

Hickman S. H., M. D., Zoback, and W. L. Ellsworth (2004), Introdcution to special section: Preparing for the San Andreas Fault Observatory at Depths, *Geophys. Res. Lett.*, *31*, L12S01. doi: 10.1029/2004GL020668.

Holdsworth, R. E., E. W. E., van Diggeln, C. J., Spiers, J. H. P., de Bresser, R. J., Walker, and L. Bowen (2011), Fault rocks from the SAFOD core samples: implications for weakening at shallow depths along the San Andreas Fault, California, *J. Struct. Geol.*, *33*, 132–144.

Hsieh, Y. P. (1989), Effects of relative humidity on the basal expansion of Mg-smectite equilibrated with ethylene glycol at low vapor pressure, *Clays and Clay Miner.*, *37*, 5,459–463.

Ikari, M., D. M., Saffer, and C. Marone (2009), Frictional and Hydrologic Properties of Clay-Rich Fault Gouge, *J. Geophys. Res.*, *114*, B05409. doi:10.1029/2008JB006089.

Ikari, M., D. M., Saffer, and C. Marone (2007), Effect of Hydration State on the Frictional Properties of Montmorillonite-based Fault Gouge, *J. Geophys. Res.*, *112*, B06423. 10.1029/2006JB004748.

Iwasaki, T., and T. Watanabe (1988), Distribution of Ca and Na ions in dioctahedral smectits and interstratified dioctahedral mica/smectite, *Clays and Clay Miner.*, *36*, 73–82.

Kinoshita, M., H., Tobin, J., Ashi, G., Kimura, S., Lallemant, E. J., Screaton, D., Curewitz, H., Masago, K. T., Moe, and the Expedition 314/315/316 Scientists (2009), Expedition 315 site C0002, Proceedings of the Integrated Ocean Drilling Program, Volume 314/315/316, Volume 314/315/316. doi:10.2204/iodp.proc.314315316.205.2011.

Klug H. P., and L. E. Alexander (1974), *X-Ray Diffraction Procedures for Polycrystalline and Amorphous Materials*, 2nd ed, John Wiley & Sons, New York, pp. 966.

Laird D. A. (2006), Influence of layer charge on swelling of smectites, *Appl. Clay Sci.*, *34*, 74–87.

Lockner D. A., C., Morrow, D., Moore, and S. Hickman (2011), Low strength of deep San Andreas fault gouge from SAFOD core, *Nature*, *472*. doi:10.1038/nature09927.

Mac Ewan, D. M. C. (1948), Complexes of clays with organic compounds. I. Complex formation between montmorillonite and halloysite and certain organic liquids, *Trans. Farad. Soc.*, *44*, 349–367.

Mooney R. W., A. G., Keenan, and L. A. Wood (1952), Adsorption of water vapour by montmorillonite. Heat of desorption and application of BET theory, *J. Am. Chem. Soc.*, *74*(6), 1367–1370.

Moore, D. M., and R. C. Reynolds Jr. (1997), *X-Ray Diffraction and the Identification and analysis of Clay Minerals*, 2nd edition, New York, Oxford University Press, pp. 378.

Moore D. E., and D. A. Lockner (2007), Friction of smectite clay montmorillonite, in *The Seismogenic Zone of Subduction Thrust Faults*, edited by T. Dixon and C. Moore, Columbia University Press, pp. 317–345.

Morrow C., J., Solum, S., Tembe, D., Lockner, and T. F. Wong (2007), Using drill cutting separates to estimate the strength of a narrow shear zone at SAFOD, *Geophys. Res. Lett.*, *34*, 11, L11301.

Mosser-Ruck R., K., Devineau, D., Charpentier, and M. Cathelineau (2005), Effects of ethylene glycol saturation protocols on XRD patterns: a critical review and discussion, *Clays and Clay Miner.*, *53*, 6, 631–638, doi: 10.1346/CCMN.2005.0530609.

Mueller-Vonmoos, M., and E. E. Kohler (1993), Geotechnik und Entsorgung, in Tonminerale und Tone, edited by J. K. And Lagaly G., Steinkopff Verlag, Darmstadt, 312–357.

Petschick R. (2010) McDiff Software Version 4.2.6, Johann Wolfgang Goethe Unviersitaet, Frankfurt am Main. http://www.geol-pal.uni-frankfurt.de/Staff/Homepages/Petschick/classicsoftware.html.

Saffer, D., L., McNeill, T., Byrne, E., Araki, S., Toczko, N., Eguchi, K., Takahashi, and the Expedition 319 Scientists (2010), Proc. IODP, 319: Tokyo (Integrated Ocean Drilling Program Management International, Inc.).

Saffer D., and C. Marone (2003), Comparison of smectite- and illite-rich gouge frictional properties: application to the updip limit of the seismogenic zone along subduction megathrusts, *Earth Plan. Sci. Lett.*, *215*, 219–235.

Schleicher A. M., B. A., van der Pluijm, and L. N., Warr (2010), Nanocoatings of clay and creep of the San Andreas fault at Parkfield, California, *Geology*, *38*, 7, 667–670.

Schleicher A. M., B. A., van der Pluijm, and L. N. Warr (2012), Chlorite-smectite clay minerals and fault behavior: New evidence from the San Andreas Fault Observatory at Depth (SAFOD) core, Lithosphere L158.1.

Tessier D., M., Dardaine, A., Beaumont, and A. M. Jaunet (1998), Swelling pressure and microstructure of activated swelling clay with temperature, *Clay Min.*, *33*, 255–267.

Tobin H., and M. Kinoshita (2006), NanTroSEIZE: the IODP Nankai Trough seismogenic zone experiment, *Sci. Drill.*, *2*, 23–27. doi: 10.2204/iodp.sd.2.06.2006.

Williams, C. F., F. V., Grubb, and S. P., Galanis, Jr., (2004), Heat flow in the SAFOD pilot hole and implications for the strength of the San Andreas fault, *Geophys. Res. Lett.*, *31*, L15S14.

Wu, F. T., L., Blatter, and H. Roberson, (1975), Clay gouges in the San Andreas fault system and their possible implications, *Pure and Appl. Geophys.*, *113*, 87–95. doi:10.1007/BF01592901.

Zoback M. D., S. H., Hickman, and B. Ellsworth (2011), Scientific drilling into the San Andreas fault zone, An overview of SAFOD's first five years, *Sci. Reports*, doi:10.2204/iodp.sd.11.02.2011.